

Renormalization of the elementary excitations in hole- and electron-doped cuprates due to spin fluctuations

D. Manske¹, I. Eremin^{1,2}, and K.H. Bennemann¹

¹*Institut für Theoretische Physik, Freie Universität Berlin, D-14195 Berlin, Germany*

²*Physics Department, Kazan State University, 420008 Kazan, Russia*

(November 13, 2018)

Extending our previous studies we present results for the doping-, momentum-, frequency-, and temperature- dependence of the kink-like change of the quasiparticle velocity resulting from the coupling to spin fluctuations. In the nodal direction a kink is found in both the normal and superconducting state while in the antinodal direction a kink occurs only below T_c due to the opening of the superconducting gap. A pronounced kink is obtained only for hole-doped, but not for electron-doped cuprates and is characteristically different from what is expected due to electron-phonon interaction. We further demonstrate that the kink structure is intimately connected to the resonance peak seen in inelastic neutron scattering. Our results suggest similar effects in other unconventional superconductors like Sr_2RuO_4 .

74.20.Mn, 74.25.-q, 74.25.Ha

I. INTRODUCTION

Elementary excitations in the cuprates are of central interest in order to learn more about the correlations and the pairing mechanism for superconductivity. For example, it is well-known that the understanding of the elementary excitations in conventional superconductors like lead as measured by tunneling spectroscopy played the crucial role in accepting the picture of electron-phonon-mediated Cooper-pairing¹⁻³. In the high- T_c cuprates one expects that due to the presence of antiferromagnetic spin fluctuations a strong renormalization of the spectral density and the corresponding energy dispersion may occur. It was shown by several groups^{4,5} that the so-called 'dip-hump' structure seen in tunneling experiments⁶ can be explained in terms of the feedback effect of superconductivity arising from the structure in the gap function $\Delta(\mathbf{k}, \omega)$. Moreover, it has been argued that this structure reflects the effective pairing interaction and points towards a spin-fluctuation-mediated Cooper-pairing. Recent developments in angle-resolved photoemission spectroscopy (ARPES) allow to study the elementary excitations directly and in much more detail. In particular, the anisotropy of the elementary excitations close to the Fermi energy in the different parts of the Brillouin Zone (BZ) are studied. This is important, since the coupling of the quasiparticles to spin fluctuations varies at different parts of the BZ. Furthermore, the understanding of the structures seen by ARPES and their doping, momentum, and temperature dependence will help to understand the role played by spin fluctuations in contrast to phonons regarding the formation of superconductivity in the high- T_c cuprates.

1. Theoretical background: Similar to the electron-phonon case, the coupling between the quasiparticles and the spin excitations should influence characteristically the energies $\omega_{\mathbf{k}}$ of the hole- or electron carriers

$$\omega_{\mathbf{k}} = \epsilon_{\mathbf{k}} + \text{Re } \Sigma(\mathbf{k}, \omega) \quad . \quad (1)$$

Here, $\epsilon_{\mathbf{k}}$ refers to the bare energy dispersion of the quasiparticles assuming no interaction with the spin excitations or phonons, *i.e.* a tight-binding energy dispersion for the CuO_2 -plane. In general, the self-energy $\Sigma(\mathbf{k}, \omega)$ results from the coupling of the particles to spin excitations, see Fig. 1 for an illustration. Obviously,

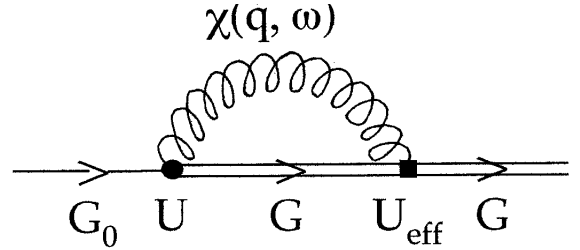


FIG. 1. Illustration of the coupling between holes or electrons and spin fluctuations characterized by the susceptibility $\chi(\mathbf{q}, \omega)$. This leads to Dyson's equation $G^{-1} = G_0^{-1} - \Sigma$ describing the relation between the bare Green's function G_0 and the renormalized one $G(\mathbf{k}, \omega)$. U (U_{eff}) denotes an effective (renormalized) coupling constant.

the self-energy is a functional of the spin susceptibility, $\Sigma = \Sigma\{\chi\}$. In its simplest form, the latter is of Ornstein-Zernicke form⁷ that allows for a sharp enhancement of fluctuations near the antiferromagnetic wave vector $\mathbf{Q} = (\pi, \pi)$:

$$\chi(\mathbf{q}, \omega) = \frac{\chi_{\mathbf{Q}}}{1 + \xi^2(\mathbf{q} - \mathbf{Q})^2 - i\frac{\omega}{\omega_{sf}}} \quad . \quad (2)$$

Here, $\chi_{\mathbf{Q}}$ is the value of the static spin susceptibility at the wave vector \mathbf{Q} , ξ is the magnetic correlation length, and ω_{sf} is the characteristic frequency of spin fluctuations (roughly the peak position in the imaginary part of Eq. (2)). Due to the fact that $\chi(\mathbf{q}, \omega)$ has only structures

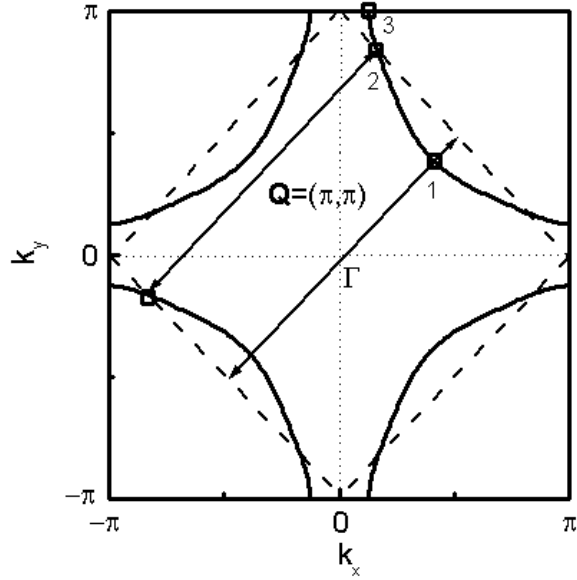


FIG. 2. Illustration of the anisotropy of the elementary excitations. The solid line denotes the calculated Fermi surface for the hole-doped cuprates in the first BZ using Eq. (3). The dashed lines refer to the magnetic Brillouin Zone that crosses the electronic Fermi surface close to the $(\pi, 0)$ points exactly at the 'hot spots' where the antiferromagnetic wave vector $\mathbf{Q} = (\pi, \pi)$ connects two pieces of the Fermi surface. At the $(\pi, 0)$ point and along the diagonal the wave vector \mathbf{Q} connects quasiparticle states below the Fermi level only. This allows us to define three characteristic regions 1,2,3 at the Fermi level.

around ω_{sf} and wave vector \mathbf{Q} , their influence on the elementary excitations is expected to be very anisotropic at different parts of the Brillouin Zone.

In order to illustrate the anisotropy of the elementary excitations we show in Fig. 2 the calculated Fermi surface for hole-doped cuprates⁸. For the calculation we use the tight-binding energy dispersion for the CuO_2 -plane

$$\epsilon_{\mathbf{k}} = -2t(\cos k_x + \cos k_y) + 4t' \cos k_x \cos k_y - \mu \quad . \quad (3)$$

Here, t and t' refer to the hopping of a hole (electron) between nearest, next-nearest sites on the square lattice, and μ is the chemical potential that defines the doping. In Eq. (3) and in the following we set the lattice constant to unity. One clearly sees that the scattering of quasiparticles by spin fluctuations in cuprates is anisotropic. First, the antiferromagnetic wave vector $\mathbf{Q} = (\pi, \pi)$ connects exactly quasiparticles at the Fermi level close to the $(\pi, 0)$ points of the first Brillouin Zone. These quasiparticles experience the strongest coupling to antiferromagnetic spin fluctuations. Quasiparticles at the diagonals of the BZ are *not* connected by the \mathbf{Q} and thus have smaller scattering by spin fluctuations at the Fermi level. The corresponding point on the Fermi surface is called *cold spot* or *nodal point*. Furthermore, the quasiparticle

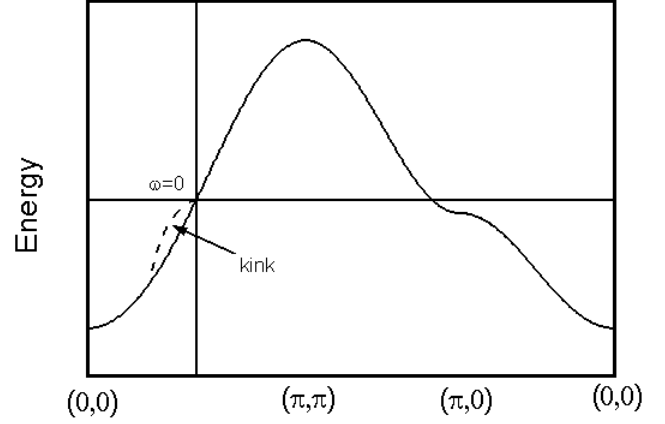


FIG. 3. Calculated bare tight-binding energy dispersion for the hole-doped cuprates in the normal state using Eq. (3). The dashed curve illustrates the changes due to renormalization, $\omega_{\mathbf{k}} = \epsilon_{\mathbf{k}} + \text{Re}\Sigma(\mathbf{k}, \omega)$. Due to structure in $\text{Re}\Sigma$ the energy dispersion shows a kink feature along the $(0, 0) \rightarrow (\pi, \pi)$ direction in the first Brillouin Zone.

states at the Fermi level close to the M point in the first BZ are usually called antinodal points. Note that the quasiparticle states at cold and hot spots which are connected by \mathbf{Q} lie *close* to the Fermi level. This will be important later for discussing the kink feature. Therefore, we may define three characteristic regions at the Fermi surface regarding their sensitivity to coupling to antiferromagnetic spin fluctuations.

2. Experimental findings: Let us now discuss the experimental situation *close* to the Fermi level as measured by ARPES. The combined study of energy distribution curves (EDC) and momentum distribution curves (MDC) allows the study of the quasiparticle excitations close and well below the Fermi level up the energies of 200 meV. Most importantly, recent ARPES studies by various groups^{10–13} reveal a kink structure in the energy dispersion at energies about $60 \pm 15 \text{ meV}$ below the Fermi energy and along the nodal direction $(0, 0) \rightarrow (\pi, \pi)$ direction of the first BZ. Furthermore, this kink structure appears in the normal state and almost does not change if one enters the superconducting state.

We illustrate the formation of the kink in Fig. 3 where we show the unrenormalized tight-binding energy dispersion $\epsilon_{\mathbf{k}}$ in the normal state along the route $(0, 0) \rightarrow (\pi, 0) \rightarrow (\pi, \pi) \rightarrow (0, 0)$ of the first BZ. Below E_f , the measured energy dispersion $\omega_{\mathbf{k}}$ along $(0, 0) \rightarrow (\pi, \pi)$ has changed compared to the bare tight-binding case due to the self-energy corrections as it follows from Eq. (1). We define the kink at the inflection point of the dashed curve where the renormalized dispersion tends to approach again the bare dispersion $\epsilon_{\mathbf{k}}$. Recent studies by Dessau and co-workers¹⁴ reveal no kink structure along $(\pi, 0) \rightarrow (\pi, \pi)$ direction in the normal state, but only in the superconducting state.

3. Doping and k-dependence of the kink: Previously we have shown¹⁵ that from the momentum and energy conservation one expects changes of the quasiparticle velocities $v_{\mathbf{k}} = \partial\epsilon/\partial\mathbf{k}$ in the nodal direction for $\omega \simeq \omega_{sf}$ and $\mathbf{k} - \mathbf{k}' = \mathbf{q} \simeq \mathbf{Q}$. This leads to the kink in the $(0,0) \rightarrow (\pi,\pi)$ direction that has been observed by angle-resolved photoemission spectroscopy (ARPES)¹⁰⁻¹³. Here, we extend our previous analysis and discuss in more detail the doping dependence and the anisotropy of the kink feature as a function of $(\mathbf{k} - \mathbf{k}_F)$ and energy $\omega_{\mathbf{k}}$ in the normal and superconducting state, for different routes $\mathbf{k} - \mathbf{k}_F$ in the Brillouin zone: $(0,0) \rightarrow (\pi,\pi)$, $(0,0) \rightarrow (0,\pi)$, and $(\pi,0) \rightarrow (\pi,\pi)$. Due to the fact that the superconducting order parameter has nodes along $(0,0) \rightarrow (\pi,\pi)$ and maxima for $(0,0) \rightarrow (0,\pi)$ one expects additional changes in the kink structure as observed recently^{16,14}. This should help to contrast renormalization due to spin fluctuations to what we get due to electron-phonon interaction. Furthermore, we investigate the interdependence of the elementary excitations with the resonance peak that is observed in hole-doped cuprates by inelastic neutron scattering (INS) below T_c . It follows also from Eq. (1) and $\text{Im}\Sigma(\mathbf{k},\omega) \propto \omega^2 \rightarrow \omega$ that the temperature dependence of the kink feature should reflect characteristically the coupling to spin fluctuations and be different from the electron-phonon coupling case.

Note that in the case of electron-doped cuprates neither a resonance peak nor a kink feature is present. We will also show that the kink feature is not restricted to the cuprates, but is also expected for other novel superconductors where quasiparticles couple strongly to spin excitations. A particularly interesting case might be Sr_2RuO_4 with large anisotropic behavior of $\chi_{zz}(\mathbf{q},\omega)$ and in-plane $\chi_{+-}(\mathbf{q},\omega)$ ^{17,18}. Generally, a strong nesting behavior of the Fermi surface might yield pronounced kink features.

This paper is organized as follow: In Section II we present the theory, and in Section III we discuss our results for the kink structure, its doping- and temperature dependence for hole- and electron-doped cuprates. Finally, in Section IV we summarize our analysis and contrast renormalization due to spin fluctuations and phonons.

II. THEORY

A. One-band Hubbard model: The elementary excitations and the spin excitations are key quantities determining the properties of the cuprates and other superconductors with strong correlations and magnetic activity. The quasiparticles, holes or electrons, interact strongly with spin fluctuations and also with phonons. However, phonons and spin fluctuations differ with respect to their doping dependence and anisotropy. This is clearly demonstrated by neutron scattering experiments,

for example. Also the different behavior of hole- and electron-doped cuprates and the feedback of superconductivity on $\chi(\mathbf{q},\omega)$ is important.

In this paper we employ an effective one-band Hamiltonian. This is justified because upon hole doping antiferromagnetism disappears due to Zhang-Rice singlet formation and quenching of Cu-spins. In this one-band picture the Coulomb interaction between the quasiparticles refers to an effective interaction (i.e. the Hubbard U) within the conduction band. Then, further doping increases the carrier mobility and a system of strongly correlated quasiparticles occurs. In the overdoped case less magnetic activity is present yielding usual Fermi liquid. We assume $U \simeq W/2$ (W = bandwidth) independent of the doping concentration.

The main physics of a single CuO_2 -plane is the two-dimensional one-band Hubbard model given by

$$H = - \sum_{\langle ij \rangle \sigma} t_{ij} (c_{i\sigma}^\dagger c_{j\sigma} + c_{j\sigma}^\dagger c_{i\sigma}) + U \sum_i n_{i\uparrow} n_{i\downarrow} \quad , \quad (4)$$

where $c_{i\sigma}^\dagger$ creates an electron with spin σ on site i , U denotes the on-site Coulomb interaction, and t_{ij} is the hopping integral. After diagonalization of the first term, one arrives at the bare tight-binding energy dispersion given by Eq. (3). The description of the electron- and hole-doped cuprates within a one-band approximation is possible if one takes into account different parameters and quasiparticle dispersion¹⁹. Note that in the case of electron doping the electrons occupy the copper d -band, while in the hole-doped case holes refer mainly to the oxygen p -states yielding different dispersion parameters. Furthermore, the energy dispersions for optimally hole-doped $\text{La}_{2-x}\text{Sr}_x\text{CuO}_4$ (LSCO) and electron-doped $\text{Nd}_{2-x}\text{Ce}_x\text{CuO}_4$ (NCCO) behave differently around $(\pi,0)$ point. While in the case of LSCO the flat band (leading to the van Hove singularity in the density of states) lies close to the Fermi level, in NCCO the flat band is approximately 300 meV below the Fermi level. Then, using $t = 250\text{meV}$ and $t' = 0.1t$, one describes the hole-doped LSCO dispersion, whereas $t = 138\text{meV}$ and $t' = 0.3t$ are needed for the description of the electron-doped NCCO compound fitting earlier photoemission data. These parameters including an intermediate coupling $U = 4t$, will be used for our calculations of various physical quantities in the normal and superconducting state of electron- and hole-doped cuprates²⁰.

B. Generalized Eliashberg equations: In this one-band model, we assume that the *same* electrons (holes) are participating in the formation of antiferromagnetic fluctuations and in Cooper-pairing due to the exchange of these fluctuations. Thus, both the magnetic susceptibility and the quasiparticle self-energy must be calculated self-consistently. This is possible in the FLEX approximation²¹⁻²⁴. In this approach the dressed one-electron Green's function are used to calculate the charge and spin susceptibilities. These susceptibilities are then

used to construct an effective Berk-Schrieffer-like²⁵ pairing interaction V_{eff} describing the exchange of charge and spin fluctuations. The generalized Eliashberg equations are derived in Appendix A. In order to demonstrate the significant role of V_{eff} in our work, we also show in Fig. 13 its corresponding diagrammatic representation. Note, in general, if the Cooper-pairing and the effective pairing potential V_{eff} are generated by the same quasiparticles (solid lines in Fig. 13), strong self-energy and feedback effects on $G(\mathbf{k}, \omega)$ and $\chi(\mathbf{q}, \Omega)$ are expected²⁶.

To be more precise, we write down the quasiparticle self-energy components Σ_ν ($\nu = 0, 3, 1$) with respect to the Pauli matrices τ_ν in the Nambu representation^{28,29}, *i.e.* $\Sigma_0 = \omega(1 - Z)$ (mass renormalization), $\Sigma_3 = \xi$ (energy shift), and $\Sigma_1 = \phi$ (gap parameter). They are given by

$$\begin{aligned} \Sigma_\nu(\mathbf{k}, \omega) = N^{-1} \sum_{\mathbf{k}'} \int_0^\infty d\Omega V_{\text{eff}}(\mathbf{k} - \mathbf{k}', \Omega) \\ \times \int_{-\infty}^{+\infty} d\omega' I(\omega, \Omega, \omega') A_\nu(\mathbf{k}', \omega') \end{aligned} \quad (5)$$

with

$$V_{\text{eff}} = [P_s(\mathbf{k} - \mathbf{k}', \Omega) - (\delta_{\nu 1} - \delta_{\nu 0} - \delta_{\nu 3}) P_c(\mathbf{k} - \mathbf{k}', \Omega)]. \quad (6)$$

This is a generalization of figure 1. P_s and P_c denote the spectral density of the spin and charge excitations, respectively, and are defined in Eqs. (A3) and (A4). The second part of Eq. (5) is given in Eqs. (A5) and (A6). It is interesting to remark that the above formulae remain valid even if the elementary excitations and the magnetic activity that controls V_{eff} would result from different quasiparticles.

The generalized Eliashberg equations allow us to calculate all the properties of the system self-consistently like superconducting phase diagram, elementary excitations, the superconducting order parameter, energy dispersion and dynamical spin susceptibility, for example^{30,9}. Note, in Eq. (5) self-energy effects due to phonons are neglected. Their contribution will be discussed in section IV and in Appendix B.

III. RESULTS AND DISCUSSION

A. Anisotropic Renormalization

1. Nodal direction: We start the discussion analyzing the spectral density of hole-doped superconductors in the normal state. The spectral density reveals the elementary excitations and in particular the renormalized energy dispersion. First, we present our results for the spectral density along the nodal $(0, 0) \rightarrow (\pi, \pi)$ direction in the first BZ.

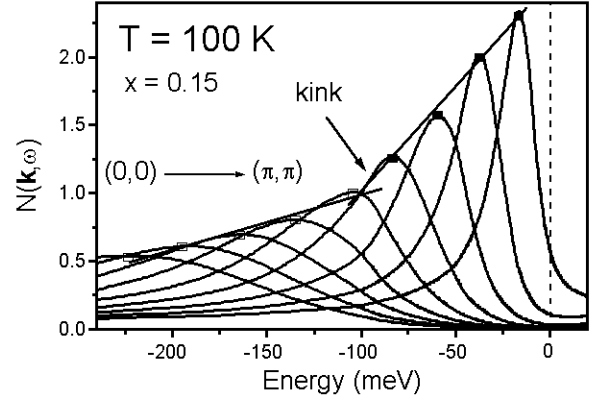


FIG. 4. Calculated spectral density $N(\mathbf{k}, \omega)$ in the normal state along the nodal $(0, 0) \rightarrow (\pi, \pi)$ direction (from left to right) as a function of frequency in the first Brillouin zone (BZ). The peak positions (connected by the solid line to guide the eye) refer to the renormalized energy dispersion $\omega_{\mathbf{k}}$. One clearly sees the kink structure at an energy approximately $\omega_{\text{kink}} = 75 \pm 15 \text{ meV}$ that results from coupling of the quasiparticles to spin fluctuations.

In Fig. 4 we show the calculated spectral density $N(\mathbf{k}, \omega)$, *i.e.* the local density of states, as a function of frequency and momentum $\mathbf{k} - \mathbf{k}_F$. The peak positions correspond to the renormalized energy dispersion. Due to coupling of holes to antiferromagnetic spin fluctuations the quasiparticle dispersion changes its slope and shows a pronounced kink feature at the energy $\omega_{\text{kink}} \approx 75 \pm 15 \text{ meV}$.

How can one understand the kink feature in a simple way? At the first glance the occurrence of a kink in the nodal direction seems to be surprising, since the main interaction of the carriers with spin fluctuations occurs at the hot spots while the kink feature is present along the diagonal of the BZ close to the cold spots. This argument, however, considers only the quasiparticles exactly at the Fermi level. Away from the Fermi level but close to it (along $(0, 0) \rightarrow (\pi, \pi)$) the quasiparticles couple strongly to spin fluctuations, as can be seen from Fig. 2. Most importantly, as follows from Fig. 2, the largest scattering will occur at values of $\mathbf{k} - \mathbf{k}_F = \mathbf{Q}$ and $\omega = \omega_{sf}$. To be more precise, let us rewrite Eq. (5) as

$$\begin{aligned} \Sigma(\mathbf{k}, i\omega_n) = -T^2 \sum_{\omega_m, \nu_m} \sum_{\mathbf{k}', \mathbf{q}} \tilde{\tau}_0 G(\mathbf{k} - \mathbf{k}', i\omega_n - i\nu_m) \tilde{\tau}_0 U^2 \\ \times \frac{1}{2} \text{Tr} [\tilde{\tau}_0 G(\mathbf{k} + \mathbf{q}, i\omega_m + i\nu_m) \tilde{\tau}_0 G(\mathbf{q}, i\omega_m)] \end{aligned} \quad (7)$$

and approximate the Green's function by its non-interacting part

$$G(\mathbf{k}, i\omega_n) \approx G_0(\mathbf{k}, i\omega_m) = \frac{i\omega_n \tilde{\tau}_0 + \epsilon_{\mathbf{k}} \tilde{\tau}_3 - \phi_{\mathbf{k}} \tilde{\tau}_1}{(i\omega_n)^2 - E_{\mathbf{k}}^2} \quad (8)$$

with $E_{\mathbf{k}}^2 = \epsilon_{\mathbf{k}}^2 + \phi_{\mathbf{k}}^2$. Thus, after little algebra one obtains on the real axis³²

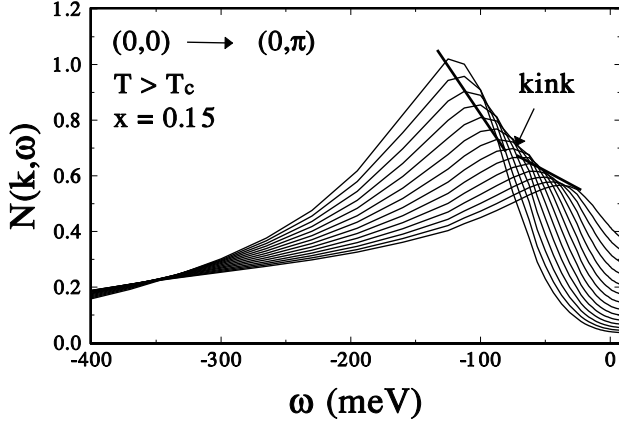


FIG. 5. Spectral density $N(\mathbf{k}, \omega)$ as a function of frequency along the $(0, 0) \rightarrow (0, \pi)$ direction of the first BZ in the normal state calculated from the generalized Eliashberg equations. Again, the peak positions reveal the renormalized energy dispersion $\omega_{\mathbf{k}}$. A kink occurs at similar energy as in the nodal direction. Because of inelastic scattering of holes on spin fluctuations close to $(0, \pi)$, $N(\mathbf{k}, \omega)$ becomes also broader. Note that, in contrast to the nodal direction, one does not cross the Fermi level in the $(0, 0) \rightarrow (0, \pi)$ direction. Instead, one reaches the flat part of the tight-binding band.

$$\Sigma(\mathbf{k}, \omega) \approx -\frac{U^2}{4} \sum_{\mathbf{k}'} \int_0^\infty d\omega' \frac{\text{Im}\chi_{\text{RPA}}(\mathbf{k} - \mathbf{k}', \omega')}{\omega - \omega' - E_{\mathbf{k}'}} \times \left[\coth\left(\frac{\omega'}{2T}\right) - \tanh\left(\frac{\omega' - \omega}{2T}\right) \right] \quad (9)$$

The imaginary part of the spin susceptibility may be obtained within the RPA and is approximately given by Ornstein-Zernicke expression (see Eq.(2)). This self-energy Σ now enters Eq. (1). It is important that the self-energy is mainly frequency-dependent, while the bare dispersion of the carriers is not. Already in the normal state, $\Sigma(\mathbf{k}, \omega)$ has a maximum reflecting a corresponding maximum of $\text{Im} \chi$ at $\mathbf{q} \approx \mathbf{Q}$ and $\omega' \approx \omega_{sf}$. Note that ω_{sf} can be determined according to Moriya and Ueda and paramagnon theory from $\chi_{\text{RPA}} = \chi_0 / (1 - U\chi_0)$ or equivalently from $\chi_0^{-1}(\mathbf{q} \simeq \mathbf{Q}, \omega \simeq \omega_{sf}) - U = 0$ ³³. Obviously, ω_{sf} is strongly doping dependent. This will be discussed later. Then, the kink position follows from the pole of the denominator of Eq. (9). This leads to the 'kink condition'

$$\omega_{\text{kink}} \approx E_{\mathbf{k}-\mathbf{Q}} + \omega_{sf}(x) \quad (10)$$

This gives an estimate of the position of the kink. Furthermore, since the superconducting gap is zero for $\omega = 0$, but not for $\omega = \omega_{sf}$, the kink feature along the nodal direction $(0, 0) \rightarrow (\pi, \pi)$ will change only slightly below T_c . This we have demonstrated previously¹⁵.

2. $(0, 0) \rightarrow (0, \pi)$ direction: In order to see whether the kink feature is present in other directions of the Brillouin Zone, we show in Fig. 5 the evolution of the spectral

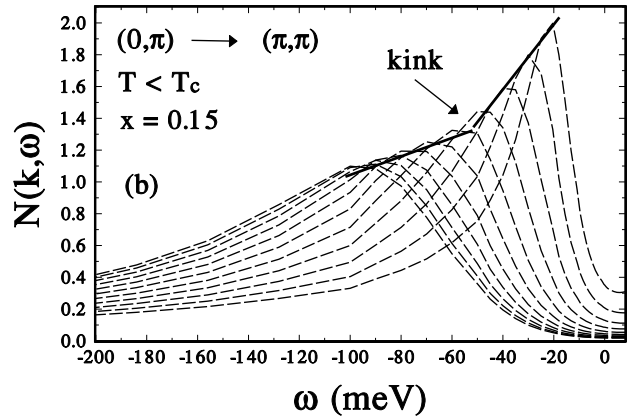
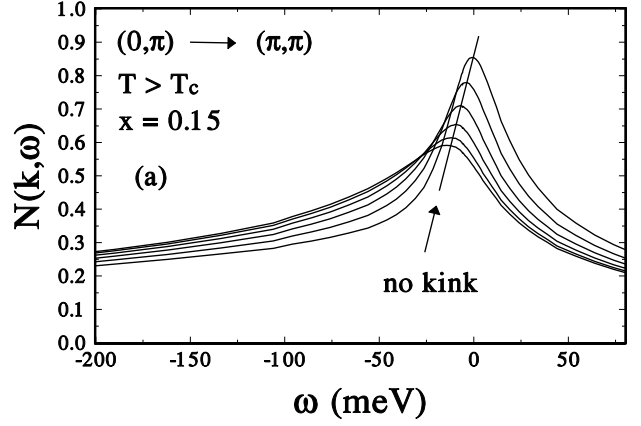


FIG. 6. Calculated spectral density $N(\mathbf{k}, \omega)$ along the antinodal $(\pi, 0) \rightarrow (\pi, \pi)$ direction as a function of frequency in the first BZ in the normal (a) and superconducting (b) state. Due to the flat band close to the Fermi level the spectral density shows no kink structure in the normal state. Below T_c the superconducting gap $\phi(\omega)$ opens yielding a kink structure in the spectral density that occurs at the energies $\omega_{\text{kink}} \approx 50 \pm 10$ meV at optimal doping.

density along the $(0, 0) \rightarrow (0, \pi)$ direction. Despite of the fact that along this direction we do not cross the Fermi level, the kink feature is still present and is found at an energy similar to the one for the nodal $(0, 0) \rightarrow (\pi, \pi)$ direction. This indicates that the occurrence of the kink feature is not connected to some specific conditions which might be present only along the $(0, 0) \rightarrow (\pi, \pi)$ direction. Instead, the kink is characteristic for all direction where $\mathbf{k} - \mathbf{k}_F \simeq \mathbf{Q}$ and $\omega \simeq \omega_{sf}$. Also below T_c we find that the kink feature is present in the $(0, 0) \rightarrow (0, \pi)$ direction (not shown). Note, that our results are in fair agreement with experimental data¹².

3. Antinodal direction: In Fig. 6(a) we show our results for $N(\mathbf{k}, \omega)$ along the $(\pi, 0) \rightarrow (\pi, \pi)$ route, i.e. the antinodal direction, of the first BZ in the normal state. Note, that the spectral density at the $(0, \pi)$ point

is broader than at the antinodal point due to stronger coupling to spin excitations peaked at $\mathbf{q} = \mathbf{Q} = (\pi, \pi)$ as discussed in Fig. 2. Clearly, no kink is present. The absence of a kink structure can be explained with the flat structure of the CuO_2 -plane around the M point (see Fig. 3). Simply speaking, for a flat band the frequency dependence of Σ in Eq. (1) does not play a significant role and therefore no change of the velocity and no kink structure is present.

What does happen in the superconducting state? Below T_c the superconducting gap $\phi(\mathbf{k}, \omega)$ opens rapidly for decreasing temperature T and becomes maximal in momentum space around the M point reflecting the momentum dependence of the effective pairing interaction (see Eq. (5)). In addition, due to the frequency dependence of the gap the flat band around M disappears.

In Fig. 6(b) we show results for $N(\mathbf{k}, \omega)$ at a temperature $T = 0.5T_c$ where the superconducting gap has opened. A kink structure around $\omega_{\text{kink}} \approx 50 \pm 10$ meV is present reflecting the magnitude of ϕ . Hence, in the $(\pi, 0) \rightarrow (\pi, \pi)$ direction this kink feature is only present below T_c and connected to the feedback effect of ϕ on the elementary excitations. We will show later that this feedback is also important for the resonance peak seen in INS.

Note, that the superconducting gap $\phi(\mathbf{k}, \omega)$ is calculated self-consistently in our theory and reflecting the underlying spin fluctuations which dominate the pairing potential V_{eff} . Therefore, the occurrence of a kink structure *only* below T_c in the antinodal direction is a direct fingerprint of the spin excitation spectrum³⁵. Furthermore, as we will discuss below, $\text{Im } \chi(\mathbf{Q}, \omega)$ entering in Eq. (9) is peaked at the resonance frequency ω_{res} (roughly at $\omega_{sf} + \Delta$). Therefore, the kink condition is given by

$$\omega_{\text{kink}} \approx E_{\mathbf{k}-\mathbf{Q}} + \omega_{\text{res}}(x) \quad . \quad (11)$$

In Fig. 7(a) the frequency dependence of $\text{Re } \Sigma(\mathbf{k}_a, \omega)$ in the normal and superconducting state at the antinodal point $\mathbf{k} = \mathbf{k}_a$ is shown. Due to the occurrence of the resonance feature in $\text{Im } \chi(\mathbf{Q}, \omega)$ and the related feedback of the superconducting gap $\phi(\omega)$, $\text{Re } \Sigma$ shows a pronounced structure below T_c at energies of about $\omega_{\text{res}} + \Delta_0$. Also the corresponding imaginary part, $\text{Im } \Sigma(\mathbf{k} = \mathbf{k}_a, \omega)$, shows a peak below T_c (see Fig. 7(b)). This pronounced behavior is responsible for the kink formation along $(\pi, 0) \rightarrow (\pi, \pi)$ direction in the BZ. Therefore, while the kink features are present along $(0, 0) \rightarrow (\pi, \pi)$ and $(\pi, 0) \rightarrow (\pi, \pi)$ directions in the superconducting state of hole-doped cuprates, their nature is qualitatively different. Along the nodal direction the superconducting gap is zero (for $\omega = 0$) and thus the feedback effect of superconductivity on the elementary and spin excitations is small. Therefore, ω_{sf} determines mainly the formation of the kink feature. On the other hand, along the antinodal direction the gap is maximal and yields a strong feedback of superconductivity on χ . Thus, in the

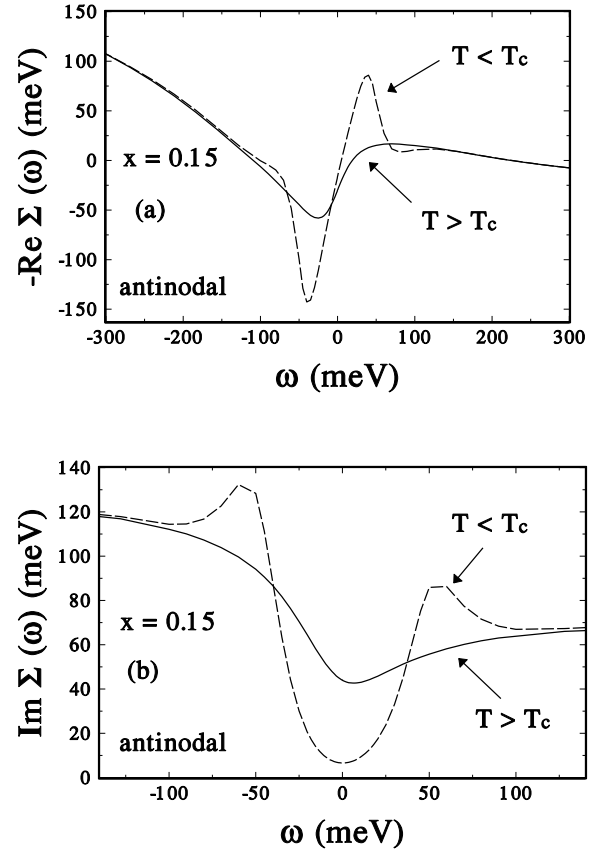


FIG. 7. (a) Calculated frequency dependence of $\text{Re } \Sigma(\mathbf{k}_a, \omega)$ at the antinodal point \mathbf{k}_a of the first BZ in the normal (solid curve) and superconducting state (dashed curve). Due to the feedback effect of the superconducting gap $\phi(\omega)$, a peak (dip) occurs for $\omega > 0$ ($\omega < 0$) which roughly defines the position of the kink structure. (b) The corresponding imaginary part at the antinodal point $\text{Im } \Sigma(\mathbf{k} = \mathbf{k}_a, \omega)$ is shown. Again, due to the feedback effect of $\phi(\omega)$, a maximum occurs below T_c . Note, that both $\text{Re } \Sigma$ and $\text{Im } \Sigma$ are not fully antisymmetric (symmetric) with respect to ω at optimum doping $x = 0.15$.

superconducting state ω_{res} and Δ_0 yield the kink structure along $(\pi, 0) \rightarrow (\pi, \pi)$ direction that is not present in the normal state.

B. Doping dependence of renormalization

The different reasons for the kink structures in hole-doped cuprates along different directions in the first BZ will be also reflected in their doping dependence. So far, the results we have shown were for optimal doping concentration $x = 0.15$ that refers to a band filling of $n = 0.85$ ³¹. Note, the superconducting transition temperature T_c behaves differently in the overdoped (OD) and underdoped (UD) regime:

$$T_c \propto \Delta(T \rightarrow 0), \text{ OD}$$

$$T_c \propto n_s(T \rightarrow 0), \text{ UD}$$

where n_s is the superfluid density that is calculated self-consistently from the generalized Eliashberg equations⁹.

In the antinodal $(0, \pi) \rightarrow (\pi, \pi)$ direction the kink is only present below T_c due to the feedback of $\phi(\omega)$. In the OD case, $\phi(\omega)$ decreases reflecting a mean-field-like behavior. Thus, the energy where the kink occurs must decrease with overdoping:

$$\omega_{kink}(x) \propto \Delta_0(x) \quad . \quad (12)$$

This behavior is indeed observed by Dessau and co-workers¹⁴. Note, the above argument remains true also in the strongly OD case where no resonance peak in $\text{Im } \chi(\mathbf{Q}, \omega)$ occurs because the feedback effect of $\phi(\omega)$ should always be present.

Regarding the kink along the nodal $(0, 0) \rightarrow (\pi, \pi)$ direction we note the following. In Fig. 8 we show the calculated doping dependence of $\text{Im } \chi$ at the antiferromagnetic wave vector \mathbf{Q} versus frequency in the normal state. One clearly sees the characteristic Ornstein-Zernicke behavior (see Eq. (2)) of $\text{Im } \chi$,

$$\text{Im } \chi(\mathbf{q} = \mathbf{Q}, \omega) \propto \frac{\omega \omega_{sf}}{\omega^2 + \omega_{sf}^2} \quad , \quad (13)$$

and that ω_{sf} increases with increasing doping from underdoped to overdoped cuprates. Since ω_{sf} determines the kink position along $(0, 0) \rightarrow (\pi, \pi)$ direction we expect

$$\omega_{kink}(x) \propto \omega_{sf}(x) \quad . \quad (14)$$

This is in qualitative agreement with experimental data¹¹ (for underdoped regime and optimally doped superconductors). On the other hand, the spectral weight of $\text{Im } \chi(\mathbf{Q}, \omega)$ decreases drastically with overdoping. Therefore, the coupling of the quasiparticles to spin fluctuations is getting much weaker in the OD case. These two competing effects seem responsible for the non-monotonic and weak doping dependence of the kink position in the nodal direction¹⁴.

In Fig. 9 we illustrate the kink feature resulting from the renormalization ($\frac{d\Sigma'}{d\omega} \sim v^* \sim (1 + \lambda)$, $v \approx v_F$) of the bare dispersion. We estimate $2 \leq \lambda \leq 3$. This renormalization is doping dependent and stronger for underdoped hole-doped cuprates. Of course, we expect that the position of the kink as well as the change of the quasiparticle velocity ($v \rightarrow v^*$) are important fingerprints of the coupling to spin fluctuations. Note, $v^* \rightarrow v$ for frequencies $\omega > \omega_{kink}$ reflects mainly the width of the peak in $\text{Im } \chi$. Important is the slope ratio v^*/v for $\omega < \omega_{kink}$.

Another important behavior concerns the asymmetry between hole and electron-doped cuprates. Note that no kink feature has been reported in the electron-doped cuprates³⁷. It is believed that the electron-phonon coupling is much more pronounced in electron-doped cuprates than in hole-doped ones. This is indicated, for

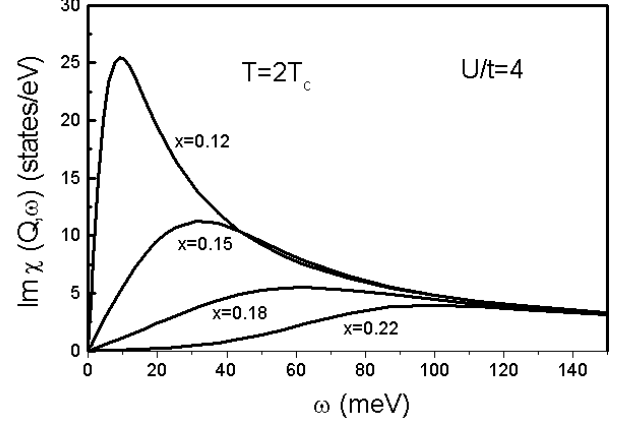


FIG. 8. Calculated paramagnon spectrum, i.e. the dynamical spin susceptibility $\text{Im } \chi(\mathbf{Q}, \omega)$ at a temperature $T = 2T_c$ for different doping concentrations, $x = 0.12$ (underdoped), $x = 0.15$ (optimal doping), and $x = 0.18, x = 0.22$ (overdoped).

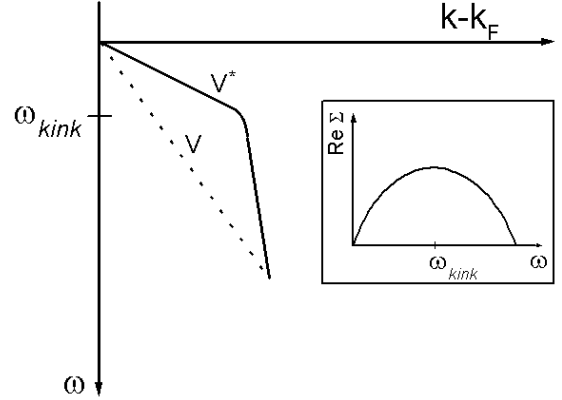


FIG. 9. Illustration of the kink position. We also show $\text{Re } \Sigma$, since this controls the kink position and v^* . The dashed curve refers to the bare dispersion. Note that $v^* \rightarrow v$ for $\omega > \omega_{kink}$ reflects mainly the width of the peak in $\text{Im } \chi$.

example, by the behavior of the resistivity $\rho \propto T^2$ in the normal state at optimum doping and by the transition between $d_{x^2-y^2}$ -wave symmetry of the superconducting gap towards anisotropic s -wave as it has been observed in several experiments³⁸. Simply speaking, the spin fluctuations in electron-doped cuprates are weaker than in the hole-doped ones yielding a smaller T_c and a smaller superconducting gap³⁹. Thus, no kink is present in the nodal direction and also no kink occurs in the $(0, \pi) \rightarrow (\pi, \pi)$ direction below T_c . This is related to the fact that the flat band around $(0, \pi)$ lies in electron-doped cuprates well below the Fermi level and, therefore, it cannot be softened due to $\phi(\omega)$.

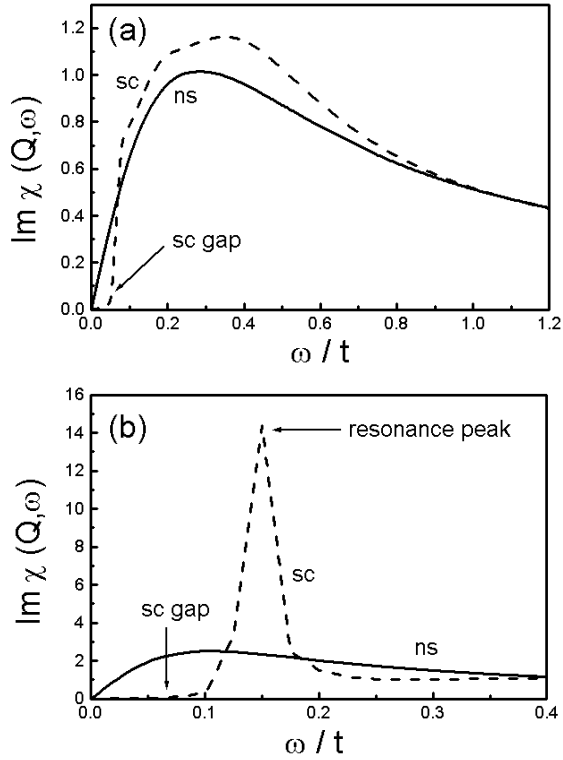


FIG. 10. Calculated feedback of superconductivity on the spin susceptibility $\text{Im } \chi(\mathbf{q}, \omega)$ for the electron-doped (a) and hole-doped (b) cuprates at optimal doping ($x=0.15$). The solid curves refer to the normal state ($T=1.5T_c$), while the dashed curves denote the renormalized spin susceptibility in the superconducting state at $T=0.7T_c$. Due to large $\omega_{sf} = 0.3t$ and the small superconducting gap, the feedback of superconductivity is small in electron-doped cuprates. Contrary, due to a small $\omega_{sf} = 0.09t$ in the hole-doped cuprates the feedback of superconductivity fulfills a resonance condition for $\text{Im } \chi$ yielding a strong renormalization of the spin excitation spectrum and to a formation of the resonance peak. Note that the hopping integral t is different for hole- and electron-doped cuprates as discussed in the introduction.

C. Relation of kink and resonance peak

In Fig. 10 we show results for the spin susceptibility $\text{Im } \chi_{RPA}(\mathbf{Q}, \omega)$ in the optimally electron(a)- and hole(b)-doped cuprates in the normal and superconducting state taking into account different tight-binding energy dispersions^{19,39}. While in the normal state of hole-doped cuprates ω_{sf} is of order of 25 meV, in the electron-doped ones its value is much larger ($\omega_{sf} \approx 70$ meV) and $\text{Im } \chi$ is much less pronounced. Therefore, antiferromagnetic spin fluctuations are much weaker in the electron-doped cuprates due to weaker nesting of the Fermi surface and less density of states due to the flat band well below the Fermi level. Regarding the superconducting state note, that in the hole-doped cuprates a strong renormalization of the spin fluctuation spectra occurs due to the

feedback effect of superconductivity and that $\Delta_0 \sim \omega_{sf}$ leading to a resonance peak at $\omega = \omega_{res}$ (see Fig. 10(b)). To be more precise, a resonance condition

$$\frac{1}{U_{cr}} = \text{Re } \chi_0(\mathbf{q} = \mathbf{Q}, \omega = \omega_{res}) \quad , \quad (15)$$

which signals the occurrence of a spin-density-wave collective mode, must be fulfilled in order to observe a resonance peak³⁵. In electron-doped cuprates, the spin excitations do not obey Eq. (15) and thus only a rearrangement of spectral weight occurs below T_c , but no resonance peak. Therefore, the kink feature is intimately connected with the resonance peak. As we see from Fig. 10(a) there is only a small feedback of superconductivity below T_c on $\text{Im } \chi$ in the electron-doped cuprates due to $\omega_{sf} \gg \Delta_0$. Thus, we find also no kink feature in the superconducting state of electron-doped cuprates in the antinodal direction.

D. Anisotropic scattering rates

Finally we discuss the anisotropy of the scattering rate $\tau^{-1}(\omega)$ of hole-doped cuprates at different points on the Fermi surface. In Fig. 11 we show our results for $\tau^{-1}(\omega)$ at the antinodal point and the nodal point, respectively, for optimal doping (a) and for the overdoped case (b) for various temperatures. In Fig. 11(a) one clearly sees that the scattering rate is very anisotropic on the Fermi surface reflecting the anisotropy of the coupling of elementary excitations to spin fluctuations. In particular, $\tau^{-1}(\omega)$ in the normal state is almost three times larger at the antinodal point than at the nodal point. This agrees with recent ARPES experiments⁴⁰. Furthermore, we find that $\text{Im } \Sigma \propto \omega$ demonstrating a non-Fermi liquid behavior in the hole-doped cuprates. Below T_c at the antinodal point $\tau^{-1}(\omega)$ reveals a strong feedback of superconductivity at energies $\omega_{res} + \Delta_0$. At the nodal point the effect of superconductivity is rather weak. In the overdoped cuprates the anisotropy between nodal and antinodal points is strongly reduced and for $\omega \rightarrow 0$ almost disappeared. Most importantly the system then behaves more Fermi-liquid-like. The latter is seen from Fig. 11(b) where one observes a crossover from the $\text{Im } \Sigma \propto \omega$ to the $\text{Im } \Sigma \propto \omega^2$ behavior. This is also in agreement with experimental observation⁴¹.

IV. SUMMARY

In summary, we have analyzed the elementary excitations in hole- and electron-doped cuprates and the fingerprints of spin fluctuations on them. The quasiparticles around the antinodal points of the BZ experience the strongest scattering on spin fluctuations yielding a non-Fermi liquid behavior. In agreement with experimental data, we find that coupling of holes to spin fluctuations

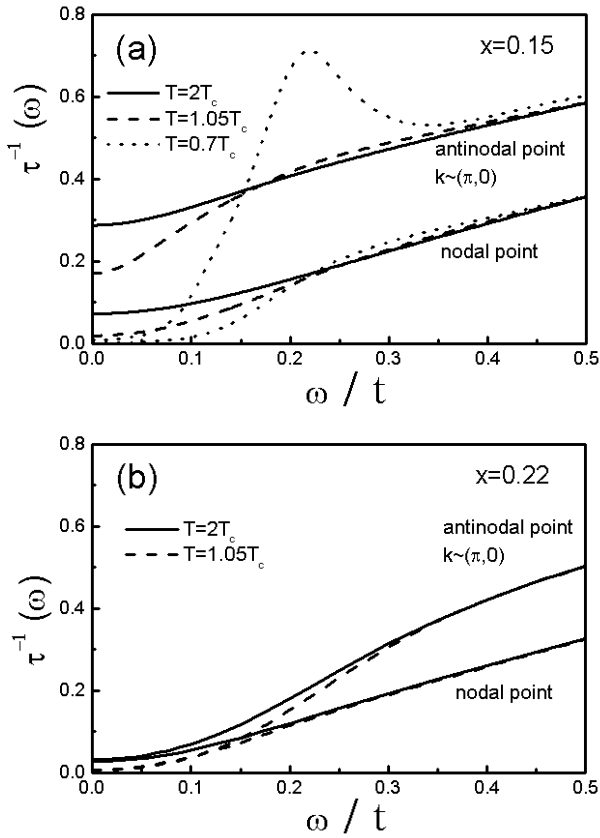


FIG. 11. Scattering rate $\tau^{-1}(\omega)$ of optimally (a) and overdoped (b) hole-doped cuprates versus frequency at the nodal and antinodal point of the Brillouin Zone (BZ) calculated at various temperatures. The anisotropy results from coupling to spin fluctuations and is disappearing in the overdoped case. Thus, a crossover from a non-Fermi liquid to a Fermi liquid behavior occurs. Note also the feedback effect of superconductivity for different parts of the BZ at optimal doping.

yields a kink feature in the renormalized energy dispersion.

Possible phonon contribution to the kink feature One of the interpretation of the kink structure in hole-doped cuprates has been the electron-phonon interaction suggested by Lanzara *et al.*¹³ Indeed, it is clear that phonons would also cause a kink structure in the energy dispersion if one assumes that Eliashberg function $\alpha^2F(\mathbf{q}, \omega)$ has the same features as $\chi(\mathbf{q}, \omega)$, namely peaked at the wave vector \mathbf{Q} and at the Debye frequency ω_D , i.e. $\omega = \omega_D \approx \omega_{sf}$. By analyzing Fig. 2 it is clear that both spin fluctuations and electron-phonon coupling can cause a kink structure. However, in general, one would expect that its position and doping dependence might be different in both cases. For example, only in the case of dominant spin fluctuation coupling the kink structure can be related to INS experiments, i.e. $\text{Im } \chi(\mathbf{Q}, \omega)$, and, furthermore, the kink position is given by $\omega_{kink} \approx E_{\mathbf{k}-\mathbf{Q}} + \omega_{sf}(x)$. As discussed earlier, the kink feature along the antinodal $(0, \pi) \rightarrow (\pi, \pi)$ direc-

tion results from the structure in $\phi(\omega)$. Thus, additional structure in $\phi(\omega)$ due to the electron-phonon interaction (EPI) may also contribute. Therefore, the question remains: How to distinguish between spin fluctuations and phonons as a reason for the kink formation? To answer this question one has to understand how consistent are both scenarios with available experimental data. For example, as was shown Zeyher and Greco³⁶, the value of electron-phonon coupling extracted from the kink analysis yields the value of the electron-phonon coupling λ and T_c that are too low to account for high- T_c superconductivity in the cuprates. Furthermore, assuming that the kink structure arises only from the EPI, it is difficult to understand the $d_{x^2-y^2}$ -symmetry of the superconducting order parameter and related observed anisotropy of the kink structure (see Appendix B). Note, only the spin fluctuation scenario yields $T_c \approx 70\text{K}$ ^{30,9}, a $d_{x^2-y^2}$ -wave order parameter, and a kink feature in qualitative agreement with experiment. Also the doping dependence of the kink is difficult to explain within the phonon scenario. In contrast to Eq. (10) one would expect $\omega_{kink} \approx E_{\mathbf{k}-\mathbf{Q}} + \omega_D(x)$ in the case of electron-phonon coupling.

Kink structure in the triplet superconductor Sr_2RuO_4 ? Finally we want to emphasize that the formation of the kink feature due to spin fluctuations should not be restricted to cuprates. For example, the quasi-two-dimensional triplet superconductor Sr_2RuO_4 (isostructural to La_2CuO_4)⁴² reveals pronounced incommensurate antiferromagnetic spin fluctuations at the wave vector $\mathbf{Q}_i = (2\pi/3, 2\pi/3)$ and frequency $\omega_{sf} \approx 6\text{meV}$ that originates from the nesting properties of the quasi-one-dimensional α and β -bands⁴³⁻⁴⁵ (see Fig. 12 for an illustration). On general grounds one would expect a kink structure in the renormalized energy dispersion of the quasiparticles. Although the correlation effects are weaker in Sr_2RuO_4 (U is smaller), and \mathbf{Q}_i is an incommensurate wave vector, similar conditions as in cuprates are present. Note, the kink feature should occur at smaller energies than in cuprates due to a lower value of ω_{sf} in the ruthenates. Further experimental studies should test our suggestion.

ACKNOWLEDGMENTS

We thank J. Fink, D. Dessau, and D. Fay for helpful discussions. The work of I. E. is supported by the 'Alexander von Humboldt' foundation and CRDF Rec.007. We further thank the DFG via the SFB 290 and INTAS (Grant No. 01-0654) for financial support.

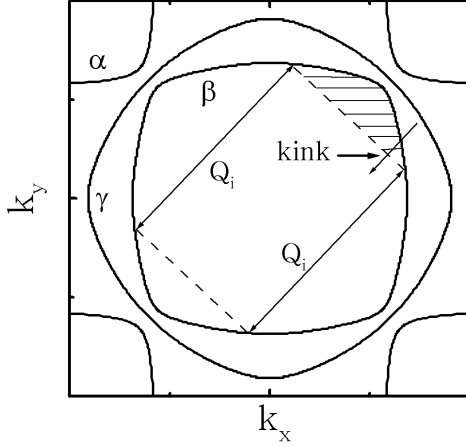


FIG. 12. Illustration of a possible kink structure in Sr_2RuO_4 . The Fermi surface of Sr_2RuO_4 consists of three bands. The nesting properties of the β -band yield to a formation of two-dimensional incommensurate spin fluctuations at $\mathbf{Q}_i = (2\pi/3, 2\pi/3)$ and $\omega_{sf} \approx 6$ meV. Therefore the quasi-particles at the β -band should be strongly renormalized due to coupling to spin fluctuations.

APPENDIX A: GENERALIZED ELIASHBERG EQUATIONS

The interdependence of elementary excitations with spin excitations leads to strong self-energy effects. The corresponding Dyson equation yields the dressed 2x2 matrix Green's function G in terms of the bare Green's function G_0 and the self-energy Σ :

$$G^{-1}(k) = G_0^{-1}(k) - \Sigma(k) \\ = i\omega_n Z(k)\tau_0 - [\epsilon(k) + \xi(k)]\tau_3 - \phi(k)\tau_1 \quad , \quad (\text{A1})$$

where $k = (\mathbf{k}, i\omega_n)$. In the FLEX approximation for the Hubbard Hamiltonian the self-energy Σ is determined by the following generalized Eliashberg equations:

$$\Sigma(k) = \sum_{k'} [P_s(k - k')\tau_0 G(k')\tau_0 + P_c(k - k')\tau_3 G(k')\tau_3] \\ = \sum_{k'} V_{\text{eff}}(k - k') G(k'). \quad (\text{A2})$$

In order to provide a better understanding of our numerical procedure we show the corresponding Feynman diagrams for V_{eff} in Fig. 13. Within RPA the spin and charge fluctuation interaction are given by

$$P_s = (2\pi)^{-1} U^2 \text{Im} (3\chi_s - \chi_{s0}) \quad , \quad (\text{A3})$$

with $\chi_s = \chi_{s0}(1 - U\chi_{s0})^{-1}$ and

$$P_c = (2\pi)^{-1} U^2 \text{Im} (3\chi_c - \chi_{c0}) \quad , \quad (\text{A4})$$

with $\chi_c = \chi_{c0}(1 + U\chi_{c0})^{-1}$. Therefore, the kernel I and the spectral functions of the one-particle Green's function in Eq. (5), A_ν , read

$$I(\omega, \Omega, \omega') = \frac{f(-\omega') + b(\Omega)}{\omega + i\delta - \Omega - \omega'} + \frac{f(\omega') + b(\Omega)}{\omega + i\delta - \Omega - \omega'}, \quad (\text{A5})$$

$$A_\nu(\mathbf{k}, \omega) = -\pi^{-1} \text{Im} [a_\nu(\mathbf{k}, \omega)/D(\mathbf{k}, \omega)], \quad (\text{A6})$$

and

$$D = [\omega Z]^2 - [\epsilon_{\mathbf{k}}^0 + \xi]^2 - \phi^2, \quad (\text{A7})$$

$$a_0 = \omega Z, \quad a_3 = \epsilon_{\mathbf{k}}^0 + \xi, \quad a_1 = \phi. \quad (\text{A8})$$

In Eq. (A5) f and b are the Fermi and Bose distribution function, respectively. Finally, the bare susceptibility is calculated from

$$\text{Im} \chi_{s0, c0} = \frac{\pi}{N} \int_{-\infty}^{\infty} d\omega' [f(\omega') - f(\omega' + \omega)] \\ \times \sum_{\mathbf{k}} [N(\mathbf{k} + \mathbf{q}, \omega' + \omega) N(\mathbf{k}, \omega') \\ \pm A_1(\mathbf{k} + \mathbf{q}, \omega' + \omega) A_1(\mathbf{k}, \omega')] \quad , \quad (\text{A9})$$

where we assume that the *same* itinerant carriers are responsible for the elementary excitations and, at the same time, generate the spin excitations. In Eq. (A9) we use $N(\mathbf{k}, \omega) = A_0(\mathbf{k}, \omega) + A_3(\mathbf{k}, \omega)$, and the real parts are calculated with the help of the Kramers-Kronig relation. The subtracted terms in P_s and P_c remove a double counting that occurs in second order. Note that V_{eff} in Eq. (5) is dominated by the exchange of spin fluctuations due to the fact that the system is in the vicinity of an antiferromagnetic phase transition, but the above equations still remain valid in the case where χ_c becomes more important.

Our numerical calculations are performed on a square lattice with 256×256 points in the first Brillouin Zone and with 200 points on the real ω -axis up to $16t$ on a logarithmic scale. Within our self-consistent procedure the full momentum and frequency dependence of quantities is kept.

APPENDIX B: PHONONS AND $\mathbf{D}_{\mathbf{x}^2-\mathbf{y}^2}$ -WAVE SUPERCONDUCTIVITY

In this Appendix we analyse how the magnetic mode which is mainly peaked at $\mathbf{q} = \mathbf{Q} = (\pi, \pi)$ leads to a $d_{x^2-y^2}$ -wave order parameter that is maximal around $(\pi, 0)$ and, in particular, to which extend phonons contribute to this result. In general, the generalized Eliashberg equations read after the inclusion of *attractive* phonons (branch i) via their spectral function $\alpha^2 F_i(\mathbf{q}, \Omega)$:

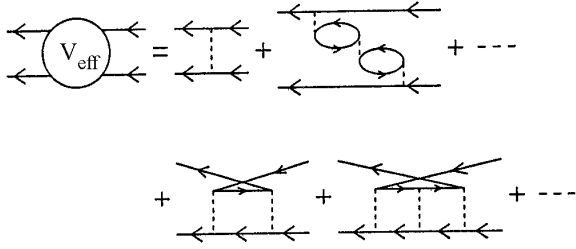


FIG. 13. Particle-particle channel of the Bethe-Salpeter equation for superconductivity due to an effective pairing interaction V_{eff} entering in Eq. (5). The solid lines refer to G and the dashed lines denote the effective Coulomb interaction U of Eq. (4). Vertex corrections that would yield to a renormalized coupling strength U_{eff} (as indicated in Fig. 1) are neglected. The summation of the corresponding bubble and ladder diagrams is performed up to infinity. While in principle it is possible to treat $V_{\text{eff}}\{\chi\}$ and $G(\mathbf{k}, \omega)$ on different levels, we assume that both quantities are generated by the *same* itinerant quasiparticles. Note, V_{eff} refers to the exchange of spin and charge fluctuations yielding a $d_{x^2-y^2}$ -wave instability of the normal state.

$$\begin{aligned} \Sigma_{\nu}^{(i)}(\mathbf{k}, \omega) = & \\ N^{-1} \sum_{\mathbf{k}'} \int_0^{\infty} d\Omega V_{\text{eff}}(\mathbf{k} - \mathbf{k}', \Omega) - \alpha^2 F_i(\mathbf{k} - \mathbf{k}', \Omega) & \\ \times \int_{-\infty}^{+\infty} d\omega' I(\omega, \Omega, \omega') A_{\nu}(\mathbf{k}', \omega') & . \end{aligned} \quad (\text{B1})$$

For $\alpha^2 F_i(\mathbf{q}, \Omega)$ we employ a Lorentzian in frequency Ω around $\Omega_0 \approx \omega_D$ (Debye frequency), and a normalized form factor $F_i(\mathbf{q})$ peaked at $\mathbf{q} = \mathbf{q}_{\text{pair}}$ as indicated in Fig. 14. The spin fluctuations that are dominating $V_{\text{eff}}(\mathbf{q}, \omega_{sf})$ are peaked at $\mathbf{q} = \mathbf{Q}_{\text{pair}}$.

It is instructive to write down the weak-coupling limit of the $\hat{\tau}_1$ -component of Eq. (B1) that reads ($T = 0$)

$$\Delta(\mathbf{k}) = - \sum_{\mathbf{k}'} \frac{[V_{\text{eff}}(\mathbf{q}) - \alpha^2 F_i(\mathbf{q})]}{2E_k} \Delta(\mathbf{k}) \quad , \quad (\text{B2})$$

where again $E_k = \sqrt{\Delta^2(\mathbf{k}) + \epsilon_k^2}$ is the dispersion of the quasiparticles in the superconducting state. Note that the contribution to the pairing potential is repulsive for spin fluctuations and attractive for phonons, respectively. In the case where no phonons would contribute to the Cooper-pairing ($\alpha^2 F_i(\mathbf{q}) = 0$), $V_{\text{eff}}(\mathbf{q})$ bridges parts of the Fermi surface where the superconducting order parameter has opposite signs. This momentum dependence of the pairing interaction is indeed required for solving Eq. (B1) and is typical for unconventional superconductivity. Note that for a repulsive and momentum-independent pairing potential, $V_{\text{eff}}(\mathbf{q}) = \text{const}$, no solution of Eq. (B1) can be obtained.

How is the kink related to the pairing mechanism? Physically speaking, the interdependence of elementary

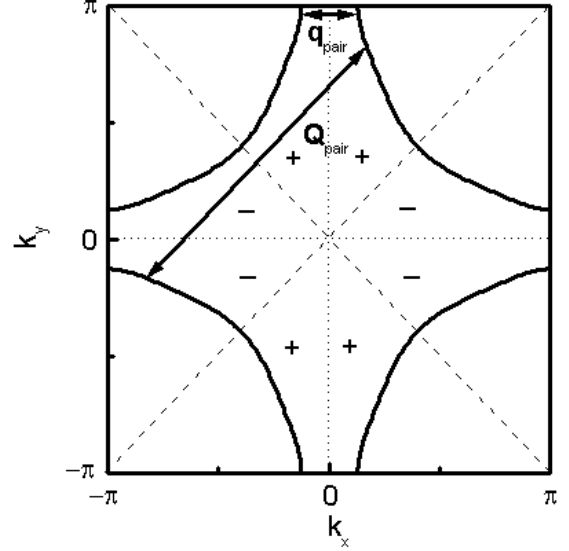


FIG. 14. Illustration of $d_{x^2-y^2}$ -wave Cooper-pairing for a fixed frequency $\Omega = \Omega_0 \approx \omega_{sf} \approx \omega_D$ due to spin fluctuations peaked at momentum $\mathbf{k} - \mathbf{k}' = \mathbf{q} = \mathbf{Q}_{\text{pair}}$ and due to phonons peaked at $\mathbf{q} = \mathbf{q}_{\text{pair}}$. The solid line denotes the Fermi surface and the dashed line refers to the nodes of the $d_{x^2-y^2}$ -wave order parameter. The corresponding sign of the order parameter is also displayed.

excitations that dominate $V_{\text{eff}}(\mathbf{q})$, leads to $d_{x^2-y^2}$ -wave Cooper-pairing as well as to the kink structure as observed by ARPES experiments. In other words, the quasiparticles around the hot spots couple strongly to spin fluctuations that leads (a) to a $d_{x^2-y^2}$ -wave order parameter, and (b) the same coupling leads to the kink in the nodal direction that occurs *close to* the Fermi level where $\mathbf{Q}_{\text{pair}} = (\pi, \pi)$ as indicated in Fig. 2.

It follows also from Eq. (14) that attractive phonons with a corresponding spectral function $\alpha^2 F(\mathbf{q})$ peaked at $\mathbf{q} = \mathbf{q}_{\text{pair}}$ contribute *constructively* to $d_{x^2-y^2}$ -wave pairing as long as the main pairing interaction is provided by spin fluctuations. However, the kink close to the antinodal points occurs *only* below T_c and is a result of $\phi(\omega)$ that is maximal around $(0, \pi)$. Therefore, the kink structure in the antinodal direction is mainly connected to spin excitations peaked at $\mathbf{Q}_{\text{pair}} = (\pi, \pi)$ and not to the phonon branch peaked at \mathbf{q}_{pair} .

Note, in the case where no spin fluctuations would be present, i.e. $V_{\text{eff}}(\mathbf{q}) = 0$, the attractive phonon contribution will cancel the minus sign on the RHS of Eq. (B1) yielding an order parameter with *s*-wave symmetry. Thus, we safely conclude that both, $d_{x^2-y^2}$ -wave Cooper-pairing and the anisotropy of the kink feature in the elementary excitations are hardly to reconcile within the same physical picture.

- ¹ J. Bardeen, L. N. Cooper, and J. R. Schrieffer, Phys. Rev. **108**, 1175 (1957).
- ² J. R. Schrieffer, D. J. Scalapino, and J. W. Wilkins, Phys. Rev. Lett. **10**, 336 (1963).
- ³ W. L. McMillan and J. M. Rowell, Phys. Rev. Lett. **14**, 108 (1965).
- ⁴ T. Dahm, D. Manske, and L. Tewordt, Phys. Rev. B **58**, 12454 (1998).
- ⁵ M. Eschrig and M. R. Norman, Phys. Rev. Lett. **85**, 3261 (2000).
- ⁶ J. F. Zasadzinski, in *Handbook of superconductivity: Conventional, High-Transition Temperature, and Novel Superconductors*, edited by K.H. Bennemann and J. B. Ketterson (Springer-Verlag, Berlin, 2002), Vol.1, p. 591.
- ⁷ A. J. Millis, H. Monien, and D. Pines, Phys. Rev. B **42**, 167 (1990).
- ⁸ We have shown in Ref. 9 that the calculated Fermi surface corresponds to an optimum doping concentration $x = 0.15$ with the highest T_c .
- ⁹ D. Manske, T. Dahm, and K. H. Bennemann, Phys. Rev. B **64**, 144520 (2001).
- ¹⁰ T. Valla, A. V. Fedorov, P. D. Johnson, B. O. Wells, S. L. Hulbert, Q. Li, G. D. Gu, and N. Koshizuka, Science **285**, 2110 (1999).
- ¹¹ P. D. Johnson, T. Valla, A. V. Fedorov, Z. Yusof, B. O. Wells, Q. Li, A. R. Moodenbaugh, G. D. Gu, N. Koshizuka, C. Kendziora, S. Jian, and D. G. Hinks, Phys. Rev. Lett. **87**, 177007 (2001).
- ¹² P. V. Bogdanov, A. Lanzara, S. A. Kellar, X. J. Zhou, E. D. Lu, W. J. Zheng, G. Gu, J.-I. Shimoyama, K. Kishio, H. Ikeda, R. Yoshizaki, Z. Hussain, and Z.-X. Shen, Phys. Rev. Lett. **85**, 2581 (2000).
- ¹³ A. Lanzara, P. V. Bogdanov, X. J. Zhou, S. A. Kellar, D. L. Feng, E. D. Lu, T. Yoshida, H. Elsaki, A. Fujimori, K. Kishio, J.-I. Shimoyama, T. Noda, S. Uchida, Z. Hussain, and Z.-X. Shen, Nature (London) **412**, 510 (2001).
- ¹⁴ A. D. Gromko, A. V. Fedorov, Y.-D. Chuang, J. D. Koralek, Y. Aiura, Y. Yamaguchi, K. Oka, Y. Ando, and D. S. Dessau, cond-mat/0202329 (unpublished).
- ¹⁵ D. Manske, I. Eremin, and K.H. Bennemann, Phys. Rev. Lett. **87**, 177005 (2001).
- ¹⁶ A. Kaminski, M. Randeria, J. C. Campuzano, M. R. Norman, H. Fretwell, J. Mesot, T. Sato, T. Takahashi, and K. Kadowaki, Phys. Rev. Lett. **86**, 1070 (2001).
- ¹⁷ Ishida, H. Mukuda, Y. Minami, Y. Kitaoka, Z. Q. Mao, H. Fukuzawa, and Y. Maeno, Phys. Rev. B **64**, 100501(R) (2001).
- ¹⁸ I. Eremin, D. Manske, and K. H. Bennemann, Phys. Rev. B **65**, 220502(R) (2002).
- ¹⁹ D. M. King, Z.-X. Shen, D. S. Dessau, B. O. Wells, W. E. Spicer, A. J. Arko, D. S. Marshall, J. DiCarlo, A. G. Loeser, C. H. Park, E. R. Ratner, J. L. Peng, Z. Y. Li, and R. L. Greene, Phys. Rev. Lett. **70**, 3159 (1993).
- ²⁰ The value $U = 4t$ makes the comparison with Refs. 9 and 15 convenient. We obtain similar results for different values of U ($3 \leq U \leq 6$).
- ²¹ N. E. Bickers, D. J. Scalapino, and S. R. White, Phys. Rev. Lett. **62**, 961 (1989); N. E. Bickers and D. J. Scalapino, Annals Phys. **193**, 206 (1989); P. Monthoux and D. J. Scalapino, Phys. Rev. Lett. **72**, 1874 (1995).
- ²² T. Dahm and L. Tewordt, Phys. Rev. Lett. **74**, 793 (1995).
- ²³ M. Langer, J. Schmalian, S. Grabowski, and K. H. Bennemann, Phys. Rev. Lett. **75**, 4508 (1995).
- ²⁴ St. Lenck, J.P. Carbotte, and R. C. Dynes, Phys. Rev. B **50**, 10149 (1994).
- ²⁵ N. F. Berk and J. R. Schrieffer, Phys. Rev. Lett. **17**, 433 (1966).
- ²⁶ This would not be the case for electron-phonon mediated Cooper-pairing due to Migdal's theorem²⁷.
- ²⁷ A. B. Migdal, Soviet Phys. JETP **1**, 996 (1958).
- ²⁸ Y. Nambu, Phys. Rev. **117**, 648 (1960).
- ²⁹ J. R. Schrieffer, *Theory of Superconductivity*, Addison-Wesley (Redwood City, 1964).
- ³⁰ D. Manske and K. H. Bennemann, Physica C **341-348**, 285 (2001).
- ³¹ The corresponding phase diagram $T(x)$ of hole-doped cuprates is shown in Fig. 3 of Ref. 9.
- ³² W. F. Brinkman and S. Engelsberg, Phys. Rev. **169**, 169 (1968).
- ³³ Note, this estimate of ω_{sf} corresponds to the peak frequency in $\text{Im } \chi$. While U controls essentially the height of the peak, its position is only weakly ω -dependent. The t -dependence of ω_{sf} is reflected by the fact that nesting gives a pronounced peak in $\text{Im } \chi$. A careful analysis of the Ornstein-Zernicke expression for the dynamical spin susceptibility (see Eq. (2)) is given by Moriya and Ueda in Ref. 34.
- ³⁴ T. Moriya and K. Ueda, Advances in Physics **49**, 555 (2000).
- ³⁵ D. Manske, I. Eremin, and K.H. Bennemann, Phys. Rev. B **63**, 054517 (2001).
- ³⁶ R. Zeyher and A. Greco, Phys. Rev. B **64**, 140510(R) (2001).
- ³⁷ Z. X. Shen, A. Lanzara, and N. Nagaosa, cond-mat/0102244 (unpublished).
- ³⁸ J. A. Skinta, T.R. Lemberger, T. Greibe, and M. Naito, Phys. Rev. Lett. **88**, 207003 (2002); J. A. Skinta, M.-S. Kim, T. Greibe, and M. Naito, *ibid*, 207005 (2002).
- ³⁹ D. Manske, I. Eremin, and K. H. Bennemann, Phys. Rev. B **62**, 13922 (2000).
- ⁴⁰ S. V. Borisenko, A. A. Kordyuk, T. K. Kim, A. Koitzsch, M. Knupfer, M.S. Golden, J. Fink, M. Eschrig, H. Berger, and R. Follath, cond-mat/0209435 (unpublished).
- ⁴¹ Z. M. Yusof, B. O. Wells, T. Valla, A. V. Fedorov, P. D. Johnson, Q. Li, C. Kendziora, S. Jian, and D. G. Hinks, Phys. Rev. Lett. **88**, 167006 (2002).
- ⁴² Y. Maeno, H. Hashimoto, K. Yoshida, S. Nishizaki, T. Fujita, J. G. Bednorz, and F. Lichtenberg, Nature (London) **372**, 532 (1994).
- ⁴³ Y. Sidis, M. Braden, P. Bourges, B. Hennion, S. Nishizaki, Y. Maeno, and Y. Mori, Phys. Rev. Lett. **83**, 3320 (1999).
- ⁴⁴ I. I. Mazin and D. J. Singh, Phys. Rev. Lett. **82**, 4324 (1999).
- ⁴⁵ D. K. Morr, P. F. Trautmann, and M. J. Graf, Phys. Rev. Lett. **86**, 5978 (2001).